Determination of the mean and the homogeneous barrier height of Cu Schottky contacts on heteroepitaxial β-Ga_2O_3 thin films grown by pulsed laser deposition

Daniel Splith[*,1], Stefan Müller[1], Florian Schmidt[1], Holger von Wenckstern[1], Johan Janse van Rensburg[2], Walter E. Meyer[2], Marius Grundmann[1]

[1] Universität Leipzig, Institut für Experimentelle Physik II, Linnéstraße 5, 04103 Leipzig, Germany
[2] University of Pretoria, Department of Physics, Lynnwood Road, Pretoria 0002, South Africa

Key words: gallium oxide, inhomogeneous Schottky barrier, heteroepitaxial thin films, pulsed laser deposition

* Corresponding author: e-mail daniel.splith@physik.uni-leipzig.de

We have investigated the electrical properties of Cu Schottky contacts on $(\bar{2}01)$-oriented β-Ga_2O_3 thin films, which have been grown by pulsed laser deposition. The I-V characteristics of two different sample structures exhibit rectification ratios at ± 2 V up to 7 orders of magnitude. The dominant current transport mechanism is thermionic emission. By fitting the I-V characteristics, we obtained the ideality factor n and the effective barrier height Φ_B^{eff} at temperatures between 50 K and 320 K. Considering a Gaussian barrier height distribution, we determined a mean barrier height of 1.32 eV. The contacts are stable at high temperatures up to at least 550 K. At this temperature a homogeneous barrier height of 1.36 eV is found, consistent with the determined mean barrier height. The ideality factor for this temperature is 1.03 and barrier inhomogeneities do not influence current transport, making the contact close to ideal.

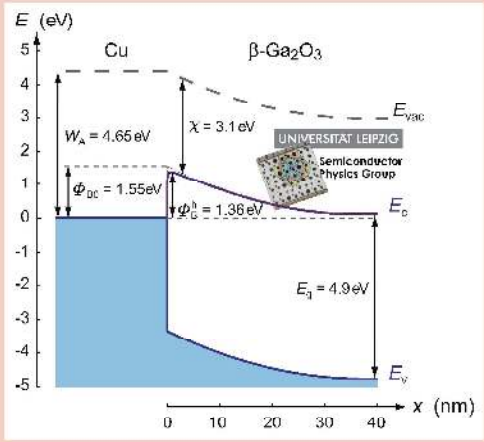

Schematic band diagram of a Cu/β-Ga_2O_3 Schottky contact at a temperature of 550 K. The inset shows a photographic image of the sample.

1 Introduction In the last years many oxide semiconductors were investigated as potential candidates for next generation opto-electronic devices. Due to its large band gap of 4.9 eV, β-Ga_2O_3 is interesting for devices like solar-blind UV-detectors, high power rectifiers or high power transistors. So far, Si or SiC with a smaller band gap of 1.1 eV or 3.3 eV are used for high power electronics. Both have, therefore, smaller theoretical breakdown fields than β-Ga_2O_3 [1]. For the development of β-Ga_2O_3-based active electronics the understanding and optimiza-

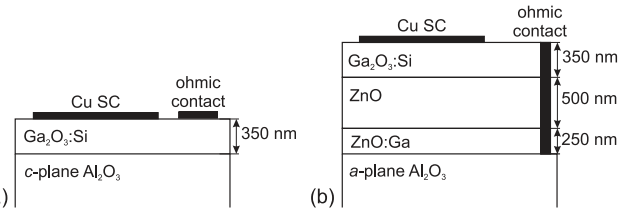

Figure 1 Layout of (a) the front-front geometry, having the SC and the ohmic contact on top of the β-Ga_2O_3 thin film on c-plane sapphire substrate, and (b) the front-back geometry, comprising the SC on top of the β-Ga_2O_3 layer and the ZnO back contact layer on a-plane sapphire substrate, acting as the ohmic back contact that is contacted from the side.

tion of unipolar devices like Schottky diodes is important. Recently, first Schottky contacts (SCs) on β-Ga_2O_3 high-quality bulk material and homoepitaxial thin films were reported [2–6]. The contact metals investigated were Au and Ni. Effective barrier heights up to $1.2\,\mathrm{eV}$ [3] and ideality factors down to 1.02 [5] had been achieved for Au SCs on β-Ga_2O_3 single crystals and effective barrier heights up to $1.1\,\mathrm{eV}$ for Ni SCs on homoepitaxial thin films. So far, the growth of β-Ga_2O_3 single crystals is a lengthy and expensive procedure and limited presently to 2" wafers [7]. Therefore, the growth of heteroepitaxial thin films on readily available substrates with large diameter and the fabrication of devices on them is a field of increasing interest. In this study we present detailed investigations on Cu SCs on heteroepitaxial grown β-Ga_2O_3 thin films on sapphire substrates.

2 Experimental All β-Ga_2O_3 thin films investigated in this study were grown by pulsed laser deposition (PLD). The laser used is a KrF excimer laser ($248\,\mathrm{nm}$) with an energy density of $2\,\mathrm{J/cm^2}$. The target-substrate distance of the setup is $10\,\mathrm{cm}$. The β-Ga_2O_3 thin films were grown from a target consisting of Ga_2O_3 and $1\,\mathrm{wt\%}$ SiO_2 at a growth temperature and oxygen partial pressure of approximately $650^\circ\mathrm{C}$ and $10^{-3}\,\mathrm{mbar}$, respectively, and were used for the fabrication of SCs within two different device layouts. For the first layout we used a front-to-front geometry, for which the β-Ga_2O_3 thin films were grown on c-plane sapphire substrates. Those thin films are single-phase and $(\bar{2}01)$-oriented as shown elsewhere [8]. The thickness of the thin films was determined by ellipsometry to be about $350\,\mathrm{nm}$. Hall effect measurements of the samples used for SCs showed that the β-Ga_2O_3 thin film is n-type with a free carrier concentration of $1.6 \times 10^{18}\,\mathrm{cm^{-3}}$, a conductivity of $0.029\,\mathrm{S\,cm^{-1}}$ and a mobility of $0.3\,\mathrm{cm^2\,V^{-1}\,s^{-1}}$ at room temperature. Due to slight changes of the PLD-process, the conductivity and the mobility of the layers are slightly increased in comparison to the thin films discussed in Ref. [8]. A scheme of the layout, which will be referred to as front-front (f-f) geometry, is depicted in Fig. 1 (a). The second layout consists of three different epilayers, allowing a front-to-back geometry. The first layer with a thickness of about $250\,\mathrm{nm}$ is a highly Ga doped ZnO layer on a-plane sapphire substrate. This highly conducting layer with an effective donor density and resistivity of $10^{21}\,\mathrm{cm^{-3}}$ and $10^{-3}\,\Omega\,\mathrm{cm}$, respectively, is used as an ohmic back-contact and ensures a low series resistance of the Schottky barrier diode [9]. The second layer is a nominally undoped ZnO layer with a thickness of about $500\,\mathrm{nm}$. This layer equilibrates the conduction band of ZnO and that of β-Ga_2O_3. Both layers are grown at a growth temperature and oxygen partial pressure of approximately $650^\circ\mathrm{C}$ and $0.016\,\mathrm{mbar}$, respectively. The top layer is a β-Ga_2O_3 thin film, deposited with the same growth parameters as used for the first sample layout. A scheme of the layout, which will be referred to as front-back (f-b) geometry, is shown in Fig. 1 (b). The crystal structure of the f-b geometry was investigated using X-ray diffraction (XRD) measurements. Those measurements were done using a Philips X'pert diffractometer with a Bragg-Brentano goniometer. The wavelength of the X-rays was $1.5406\,\text{Å}$ (Cu $K_{\alpha 1}$). Due to the highly conducting ZnO layer, Hall effect measurements of the β-Ga_2O_3 thin films were not possible, but we suppose values similar to the f-f geometry. The thickness of the β-Ga_2O_3 thin film is similar to the thickness of the thin film in the f-f geometry. Before the preparation of the SC we cleaned the surface with acetone. Using a photolithography mask, circular contacts with diameters between 150 and $750\,\mu\mathrm{m}$ were defined (see inset of the title figure). The SCs were realized by dc-sputtering of Cu in an argon atmosphere. The ohmic contacts for the f-f geometry consist of an evaporated layer structure of Ti and Al with a thickness of $25\,\mathrm{nm}$ as suggested by Villora *et al.* [10]. To ensure an ohmic behaviour and neglectable contact resistance for the ohmic contacts, it was necessary to anneal them for $10\,\mathrm{min}$ at $500^\circ\mathrm{C}$ under nitrogen ambient ($800\,\mathrm{mbar}$), as reported by Suzuki *et al.* [3]. Therefore, the ohmic contacts were realized prior to the SCs. The Cu SCs were investigated with I-V, capacitance-voltage (C-V) and capacitance-frequency measurements at room temperature. Additionally, for selected diodes temperature-dependent I-V measurements were performed. The I-V characteristics were recorded using an Agilent 4155C precision semiconductor parameter analyzer. C-V measurements were performed with an Agilent 4294A precision impedance analyzer.

3 Results and discussion Figure 2(a) depicts the I-V-characteristic of a Cu/Ga_2O_3 SC prepared on a β-Ga_2O_3 thin film (f-f geometry) at room temperature. The graph shows the I-V data for a sweep from negative to positive voltages and a reversed sweep, as indicated by arrows. The characteristic exhibits a strong exponential slope in forward direction up to $0.6\,\mathrm{V}$. For higher voltages the diode is under flat-band condition and the current flow is determined by the series resistance of the SC. In backward direction we see a slight increase of current flow, which

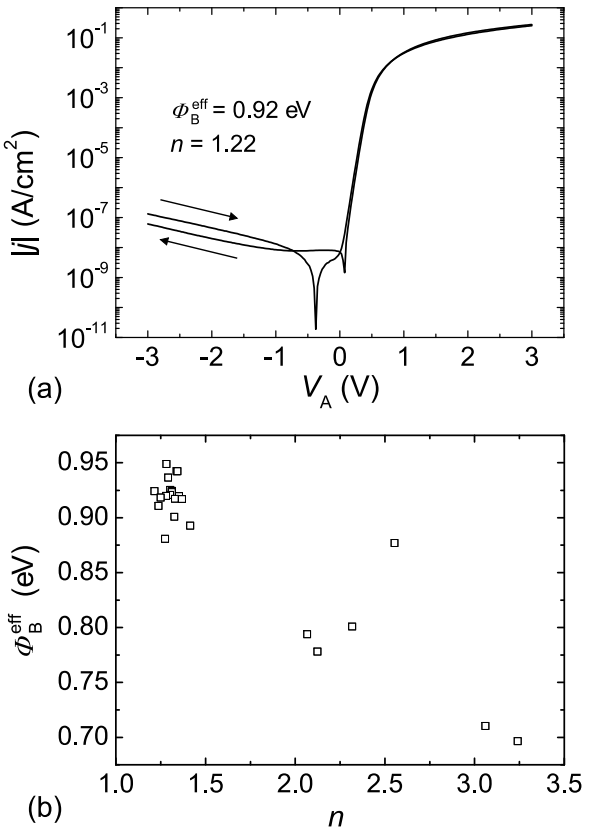

Figure 2 (a) Current density vs. applied voltage at room temperature of a Cu/Ga_2O_3 SC prepared in f-f geometry. The arrows indicate the measurement direction. (b) Effective barrier height in dependence on the ideality factor of SCs with f-f geometry.

is probably caused by barrier height inhomogeneities, as discussed below. The I-V-characteristic exhibits a strong rectifying behaviour; the rectification ratio ($\pm 2\,\mathrm{V}$) is close to 10^7 and with that among the largest reported values of SCs fabricated on β-Ga_2O_3. Since the mobility of the β-Ga_2O_3 thin films is quite low, the role of the different transport mechanisms, especially thermionic emission theory (TE) and diffusion theory, has to be discussed. Similar to [11], we calculated the difference between the effective barrier height of the combined model of thermionic emission and diffusion proposed by Crowell and Sze [12] and the effective barrier height for the model of TE with the same saturation current as in the combined model. At room temperature, for a mean barrier height of $1.3\,\mathrm{eV}$ and a standard deviation of $0.13\,\mathrm{eV}$, as determined from the temperature dependent measurements described below, this difference is about $0.011\,\mathrm{eV}$ for β-Ga_2O_3, using the mobility and the free carrier concentration determined by Hall effect measurements. This means that diffusion plays a minor role for charge transport. Therefore, TE is assumed to be the dominating transport mechanism and used to determine the effective barrier height ($\Phi_\mathrm{B}^\mathrm{eff}$) and the ideality factor (n) according to

$$I = I_\mathrm{s}\left[\exp\left(\frac{e\,(V_\mathrm{A} - IR_\mathrm{s})}{nk_\mathrm{B}T}\right) - 1\right] + \frac{V_\mathrm{A} - IR_\mathrm{s}}{R_\mathrm{p}}\,, \quad (1)$$

where e is the elementary charge, V_A the applied voltage, T the absolute temperature and k_B Boltzmann's constant. This model includes the voltage dependence of the barrier via the ideality factor n and the series and parallel resistances R_s and R_p of the diode. The saturation current I_s is given by

$$I_\mathrm{s} = A_0 A^* T^2 \exp\left(\frac{-e\Phi_\mathrm{B}^\mathrm{eff}}{k_\mathrm{B}T}\right)\,, \quad (2)$$

where A^* is the Richardson constant, with a value of $40.8\,\mathrm{A\,cm^{-2}\,K^{-2}}$ (using $m_\mathrm{e}^* = 0.34\,m_{\mathrm{e},0}$ [13]) and A_0 is the area of the contact.

Using this theory, we determined the effective barrier height and ideality factor to be $0.92\,\mathrm{eV}$ and 1.22, respectively. The effective barrier height is similar to formerly reported values of Au SCs on Czochralski grown β-Ga_2O_3 single crystals [5], even though the work function of Cu is $0.4\,\mathrm{eV}$ smaller than that of Au. The ideality factor of this contact is larger compared to SCs on single crystals. This behaviour is caused by barrier height inhomogeneities which increase the ideality factor and lower the effective barrier height as initially evoked for Si [14] and also found for SCs on ZnO [11]. The back and forward direction show a small splitting of the current zero-crossing. Such a behaviour is likely due to the charging and discharging of a parallel capacitance during the sweep measurement. Figure 2(b) summarizes the effective barrier height vs. ideality factor of several Cu/Ga_2O_3 SCs on a sample with f-f geometry. We see an accumulation of high quality SCs with an effective barrier height between $0.88\,\mathrm{eV}$ and $0.95\,\mathrm{eV}$ and ideality factor in the range of 1.2 to 1.4. However, some of the SCs have also effective barrier heights below $0.8\,\mathrm{eV}$ and ideality factors above 2. Because of the variation of the pairs of ideality factors and barrier heights for the different contacts, a linear fit for obtaining the homogeneous barrier height like expected for TE over an inhomogeneous barrier [15] is not reasonable.

The series resistance of our Cu/Ga_2O_3 prepared SCs on samples with f-f geometry is about $10\,\mathrm{k\Omega}$. For ac defect spectroscopic methods like DLTS, operating frequencies in the MHz range are required and, therefore, a reduction of the series resistance is necessary [9]. Since the sapphire substrate is insulating, we made use of a highly conductive ohmic back contact layer. For that we developed a layer structure consisting of a highly Ga doped, (00.1)-oriented ZnO layer grown on a-plane sapphire substrates. So far it was reported that β-Ga_2O_3 grows $(\bar{2}01)$-oriented on c-plane sapphire substrates [16–19], GaN substrates [20] and a-plane sapphire substrates [19]. Because of a similar structure of GaN and ZnO we expect also a $(\bar{2}01)$-oriented growth on (00.1)-oriented ZnO. Figure 3(a)

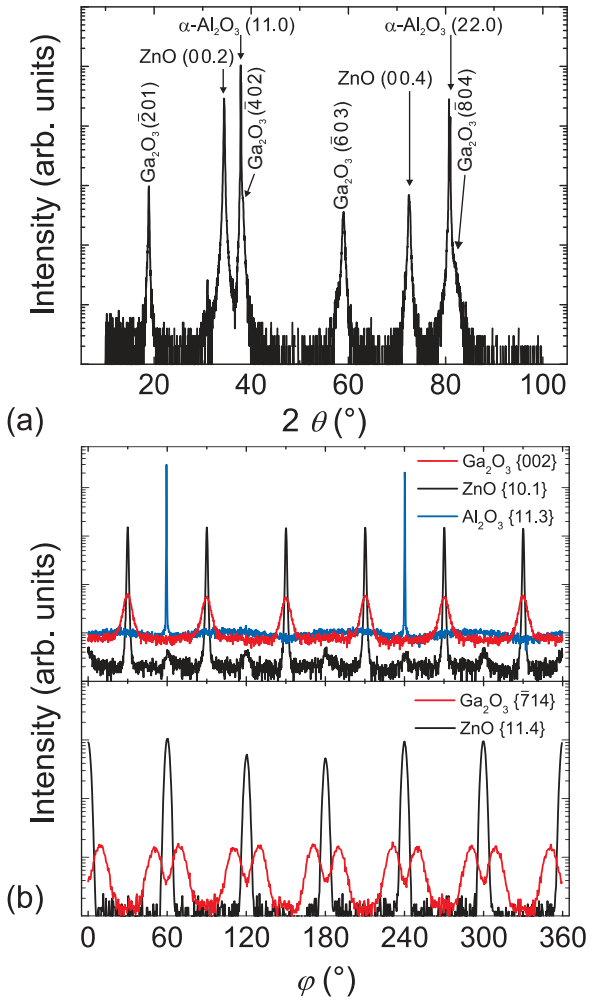

Figure 3 (a) 2θ-ω X-ray scan and (b) φ X-ray scans of a sample with f-b geometry consisting of a ZnO:Al, ZnO and β-Ga_2O_3 layers grown on a-plane sapphire substrate. The upper part shows a scan of the β-Ga_2O_3 $\{002\}$ peak, the ZnO $\{10.1\}$ peak and the sapphire $\{11.3\}$ peak, while the lower part shows a φ scan of the β-Ga_2O_3 $\{\bar{7}14\}$ peak and the ZnO $\{11.4\}$ peak. Note that the integration time of each of the scans is different for better comparability.

depicts a wide angle XRD scan of a sample with f-b geometry. The peaks occurring at angles of $34.4°$ and $72.6°$ correspond to the (00.2) and (00.4) planes of ZnO, respectively. The peaks visible at $37.8°$ and $80.8°$ are the (11.0) and (22.0) reflections of the a-plane sapphire substrate, respectively. The orientation of the β-Ga_2O_3 thin films is indicated by the occurrence of the peaks at $18.9°$, $38.4°$, $59.2°$ and $82.2°$ which correspond to the $(\bar{2}01)$, $(\bar{4}02)$, $(\bar{6}03)$ and $(\bar{8}04)$ planes of β-Ga_2O_3, respectively. Therefore, the thin films grown on ZnO have the same orientation as for growth on GaN or c-plane sapphire. The $(\bar{4}02)$ and $(\bar{8}04)$ peaks are only visible as shoulders of the (110) and (220) a-plane sapphire planes signal. Beside the mentioned ZnO, a-plane sapphire and β-Ga_2O_3 peaks no other peaks are visible. Thus, the β-Ga_2O_3 thin films are single phase with an out-of-plane orientation of $(\bar{2}01)$. In the upper part of Fig. 3(b) a φ scan of the β-Ga_2O_3 $\{002\}$ peak, the ZnO $\{10.1\}$ peak and the sapphire $\{11.3\}$ peak is shown. In accordance to literature [21], the scan shows that the $\langle 11.0\rangle$ direction of ZnO lies parallel to the $\langle 00.1\rangle$ direction of the a-plane sapphire substrate, since there is a $30°$ offset between the ZnO $\{10.1\}$ peak and the sapphire $\{11.3\}$ peak. The additional peaks in the φ scan of ZnO are due to a small amount of $30°$ rotational domains of the ZnO, which are beyond the scope of this paper. Further, the scan reveals that the $\langle 102\rangle$ direction of the $(\bar{2}01)$ oriented β-Ga_2O_3 lies parallel to the $\langle 10.0\rangle$ direction of the (00.1) oriented ZnO, since the peaks of the ZnO $\{10.1\}$ planes and the β-Ga_2O_3 $\{002\}$ planes are aligned. The fact that there are six peaks of the β-Ga_2O_3 in the φ scan means that the $\langle 102\rangle$ direction of β-Ga_2O_3 can also lie parallel to $\langle \bar{1}0.0\rangle$ direction of ZnO, since similar measurements of β-Ga_2O_3 on a c-plane ZnO single crystal also showed six peaks. According to [22], this is the minimum number of rotational domains expected for growth on c-plane ZnO. Further, the six rotational domains can be explained by the fact that the first layer of c-plane ZnO has the point group $6mm$ and the $(\bar{2}01)$ oriented β-Ga_2O_3 has the point group m and that the mirror planes of the ZnO and the β-Ga_2O_3 are aligned [23]. Diagrams of the epitaxial relation are shown in Fig. 4 (a) and (b). The lattice mismatch for $(\bar{2}01)$ oriented β-Ga_2O_3 on (00.1) ZnO are 6.6% and 30.5% in [010] direction and in [102] direction, respectively. In the lower part of Fig. 3(b) an additional φ scan of the $\{\bar{7}14\}$ peak of β-Ga_2O_3 and the $\{11.4\}$ peak of ZnO is shown. The peaks of $\{\bar{7}14\}$ planes of β-Ga_2O_3 are about $9°$ to the left and $9°$ to the right of the six peaks of ZnO. The occurrence on both sides of the peaks of ZnO can be explained by the mirror symmetry of β-Ga_2O_3. Since the mirror plane is in the b-plane, the $(\bar{7}14)$ planes are equivalent to the $(\bar{7}\bar{1}4)$ planes. Therefore, in the φ scan, both reflexes are visible. In a relaxed β-Ga_2O_3 crystal, the angle between the projection of the normal of the $(\bar{7}14)$ plane on the $(\bar{2}01)$ plane and the $[010]$ direction is $12.40°$. Nevertheless, calculating the same angle for β-Ga_2O_3 that takes the in-plane lattice parameters of ZnO (11.257 Å in [102] direction and 3.250 Å in [010] direction) yields an angle of $8.95°$, which is in accordance to the angle measured in the φ scan.

Figure 5(a) depicts the temperature-dependent I-V characteristics of a Cu/Ga_2O_3 SC with f-b geometry in the temperature range between 50 K and 320 K. The current for a given voltage increases with increasing temperature as expected for TE. For high temperature an ohmic shunt in backward direction of the I-V-characteristics is visible. At low forward voltages the I-V-characteristics are also influenced by this ohmic shunt (cf. dashed line in Fig. 5(a)). For voltages between 0.4 V and 1 V the I-V-characteristics exhibit an exponential slope for temperatures between 140 K

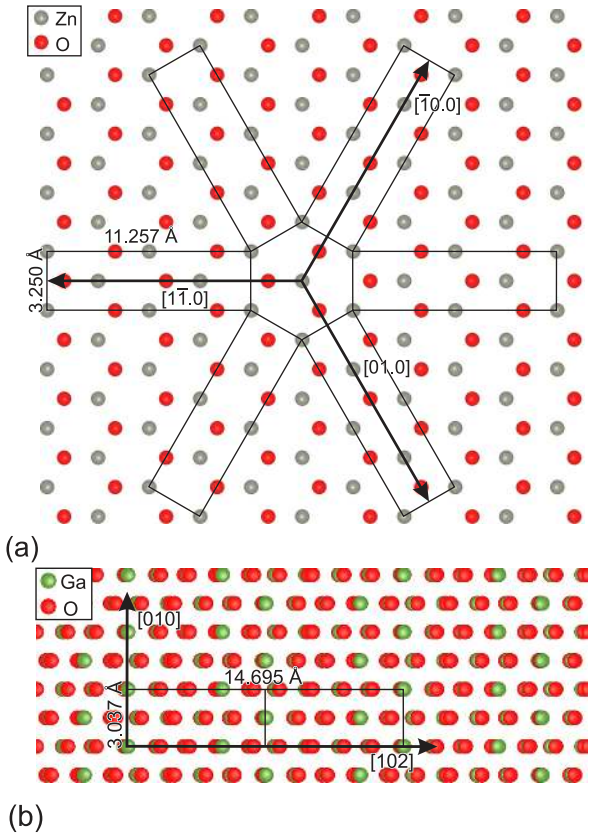

Figure 4 Schematic diagrams of the epitaxial relation between (a) (00.1)-oriented ZnO and (b) $(\bar{2}01)$-oriented β-Ga_2O_3. Both diagrams were created using VESTA [24].

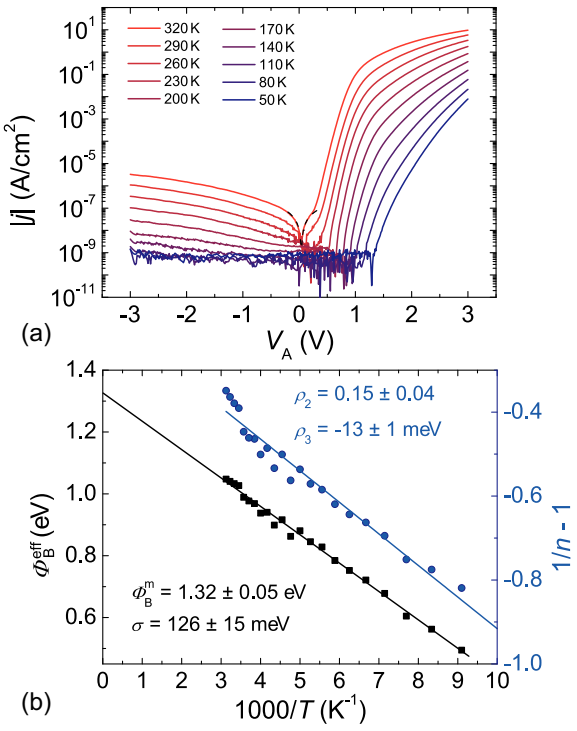

Figure 5 (a) Temperature-dependent current density voltage measurement of a Cu/Ga_2O_3 SC with f-b geometry from 50 K to 320 K. The dashed line indicates the influence of the shunt resistance for the measurement at $T = 320$ K. (b) Effective barrier height and $1/n - 1$ determined from the temperature-dependent current voltage measurement in dependence on the inverse temperature.

and 320 K. For higher voltages the barrier is under flat band conditions and the I-V-characteristics are dominated by the series resistance of the β-Ga_2O_3 and the ohmic back contact. The effective barrier height Φ_B^{eff} and ideality factor n of the depicted SC determined by TE at 290 K are 1.03 eV and 1.64, respectively. The series resistance of such SCs is now significantly reduced by nearly two orders of magnitude. For the SC shown in Fig. 5(a) the series resistance at room temperature is about 250 Ω. Figure 5(b) shows the effective barrier heights and $1/n - 1$ in dependence on the inverse temperature for temperatures above 110 K. Both the effective barrier height and $1/n - 1$ exhibit a linear dependence on the inverse temperature, which is explainable with a Gaussian distributed lateral inhomogeneous barrier height [14]. The effective barrier height is related to the mean barrier height by [14]

$$\Phi_B^{eff}(T) = \Phi_{B0}^{m} - \frac{\sigma_0^2}{2k_B T}\ , \tag{3}$$

where Φ_{B0}^{m} is the mean barrier height and σ_0 the standard deviation of the barrier height, both at zero applied bias. The change of the ideality factor with temperature can be explained by a linear dependence of the mean barrier height and the square of the standard deviation on the applied bias [14]

$$\Phi_B^{m} = \Phi_{B0}^{m} + e\rho_2 V_A \tag{4}$$

$$\sigma^2 = \sigma_0^2 + e\rho_3 V_A\ , \tag{5}$$

where ρ_2 and ρ_3 are the constants of proportionality of the mean barrier height and the square of the standard deviation, respectively. With this, the equation

$$n = \left(1 - \rho_2 + \frac{\rho_3}{2k_B T}\right)^{-1} \tag{6}$$

applies for the ideality factor [14]. Using Eq. (3) a linear fit of the effective barrier height yields a mean barrier height of 1.32 ± 0.05 eV and standard deviation of 126 ± 10 meV. A linear fit of $1/n - 1$ yields $\rho_2 = 0.15 \pm 0.04$ and $\rho_3 = -13 \pm 1$ meV.

For further investigation of the Schottky barrier at the Cu/Ga_2O_3 interface, we also measured I-V-characteristics at elevated temperatures. In Fig. 6 the I-V-characteristics of another Cu/Ga_2O_3 SC with f-b geometry is depicted for a temperature of $T = 550$ K. Again, an exponential slope

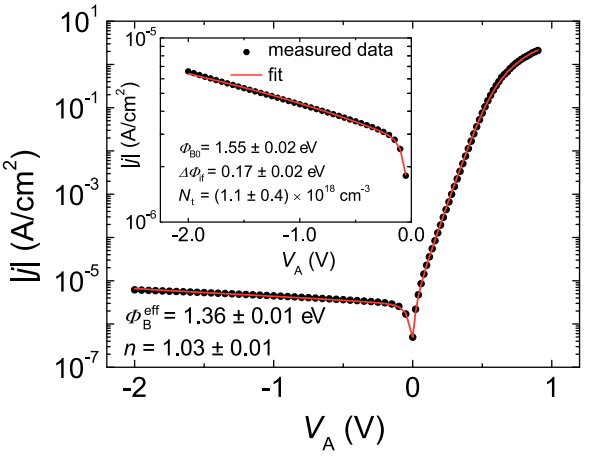

Figure 6 Current density vs. applied voltage characteristics at a temperature of $T = 550\,\mathrm{K}$ of a Cu/Ga_2O_3 SC for a sample with f-b geometry and fit of the measured data using thermionic emission theory. The inset shows a fit of the measured data for negative voltages with the model of thermionic emission considering the image force lowering of the barrier.

exists in forward direction up to $0.6\,\mathrm{V}$. For higher voltages the current transport is dominated by the series resistance of the SC, which is $50\,\Omega$ at this temperature. By fitting, we obtained an effective barrier height and an ideality factor of $1.36\,\mathrm{eV}$ and 1.03, respectively. Estimating the ideality factor for a homogeneous barrier due to image charge effects [25] yields an ideality factor of about $n_{\mathrm{if}} = 1.02$ for β-Ga_2O_3. Therefore, the ideality factor of the SC at $T = 550\,\mathrm{K}$ is close to the ideality factor expected for a homogeneous barrier, which implies that the effective barrier height for this temperature coincides with the homogeneous barrier height. Thus, both the homogeneous barrier height determined at high temperatures and the mean barrier height deduced from the temperature-dependent measurement at low temperatures ($110\,\mathrm{K}$-$320\,\mathrm{K}$) are in good agreement with each other. Additionally, the inset of Fig. 6 depicts the measured I-V characteristics for negative applied voltages in more detail. In this range, the current density depends exponentially on the applied voltage which can be seen by the linear behaviour in the semilogarithmic plot. This indicates that image charge effects like the image force lowering of the barrier is dominant for the measured characteristic. According to [26], the lowering of the Schottky barrier due to image charges is

$$\Delta\Phi_{\mathrm{if}} = e\left[\frac{e^2 N_{\mathrm{t}}}{8\pi^2\epsilon_{\mathrm{s}}\epsilon_{\infty}^2\epsilon_0^3}\left(\Phi_{\mathrm{B0}} - eV_{\mathrm{n}} - eV_{\mathrm{A}} - k_{\mathrm{B}}T\right)\right]^{\frac{1}{4}}, \tag{7}$$

where N_{t} is the net doping concentration, ϵ_0 is the vacuum permittivity, Φ_{B0} is the barrier height without the image force lowering, $eV_{\mathrm{n}} = k_{\mathrm{B}}T\left(\ln N_{\mathrm{c}} - \ln N_{\mathrm{t}}\right)$ the energy difference between the Fermi level and the conduction band and N_{c} the conduction band density of states. The latter can be calculated by [25]

$$N_{\mathrm{c}} = 2\left(\frac{m_{\mathrm{e}}^* k_{\mathrm{B}}T}{2\pi\hbar^2}\right)^{\frac{3}{2}}, \tag{8}$$

where $\hbar$ is the reduced Planck constant. At this temperature, the value of N_{c} is about $1.2 \times 10^{19}\,\mathrm{cm}^{-3}$ for β-Ga_2O_3. ϵ_{s} and ϵ_{∞} are the static and the optical dielectric constants, which are 10 and 3.61 for β-Ga_2O_3, respectively [27]. Inserting $\Phi_{\mathrm{B}}^{\mathrm{eff}} = \Phi_{\mathrm{B0}} - \Delta\Phi_{\mathrm{if}}$ into Eq. (1) and fitting the measured data with this equation gives the fit shown in the inset of Fig. 6. For this fit the ideality factor goes down to 1, which, in addition to the good agreement of the measured data with the fit, shows that there are no additional effects increasing the ideality factor. The barrier height without the image force lowering, the image force lowering and the net doping density are determined by the fit to be $1.55 \pm 0.02\,\mathrm{eV}$, $0.17 \pm 0.02\,\mathrm{eV}$ and $(1.1 \pm 0.4) \times 10^{18}\,\mathrm{cm}^{-3}$, respectively. Calculating the lowered barrier with those values gives a barrier height of $1.38 \pm 0.04\,\mathrm{eV}$, which is in good agreement with the effective barrier height determined previously from the forward characteristics. Using the work function of Cu ($W = 4.65\,\mathrm{eV}$ [28]), we can estimate the electron affinity χ of β-Ga_2O_3 to be $3.1\,\mathrm{eV}$. The deviation of this value from the electron affinity determined in [5] might be due to surface states, but this is beyond the scope of this letter. Calculating the energy difference eV_{n} between the Fermi level and the conduction band yields a value of $0.11\,\mathrm{eV}$ at a temperature of $550\,\mathrm{K}$. Therefore, according to [25], the built-in voltage V_{bi} is $1.44\,\mathrm{V}$ and the width of the space charge region w is $37\,\mathrm{nm}$. With the determined values the calculation of the schematic band diagram of a Cu Schottky contact on β-Ga_2O_3 at this temperature is possible, which is shown in the title figure.

Due to the ohmic back contact layer, the low series resistance of the SCs with a f-b geometry allows us to perform measurements of the capacitance and the conductance up to frequencies of $1\,\mathrm{MHz}$ and above. The capacitance and conductance in dependence on the measurement frequency of the SC shown in Fig. 5(a) are depicted in Fig. 7(a). In the range between $f = 1\,\mathrm{kHz}$ and $f = 100\,\mathrm{kHz}$ there is a slight decrease of the capacitance which might be due to a continuous distribution of defects states like surface states or defects states at grain boundaries. Additionally, at a frequency of about $1\,\mathrm{MHz}$ there is an inflection point indicating that the frequency matches the emission rate of a defect. Therefore, we can estimate the emission rate of this defect to be about $3\,\mathrm{MHz}$ at room temperature. Comparison with emission rates of defects discussed in [4] gives no accordance, hence, this must be a different defect. As the frequency increases further, the capacitance decreases and the conductance increases. This is the expected behaviour of a SC due to its low-pass characteristics.

In Fig. 7(b) the capacitance is depicted in dependence on the applied voltage for measurement frequencies of

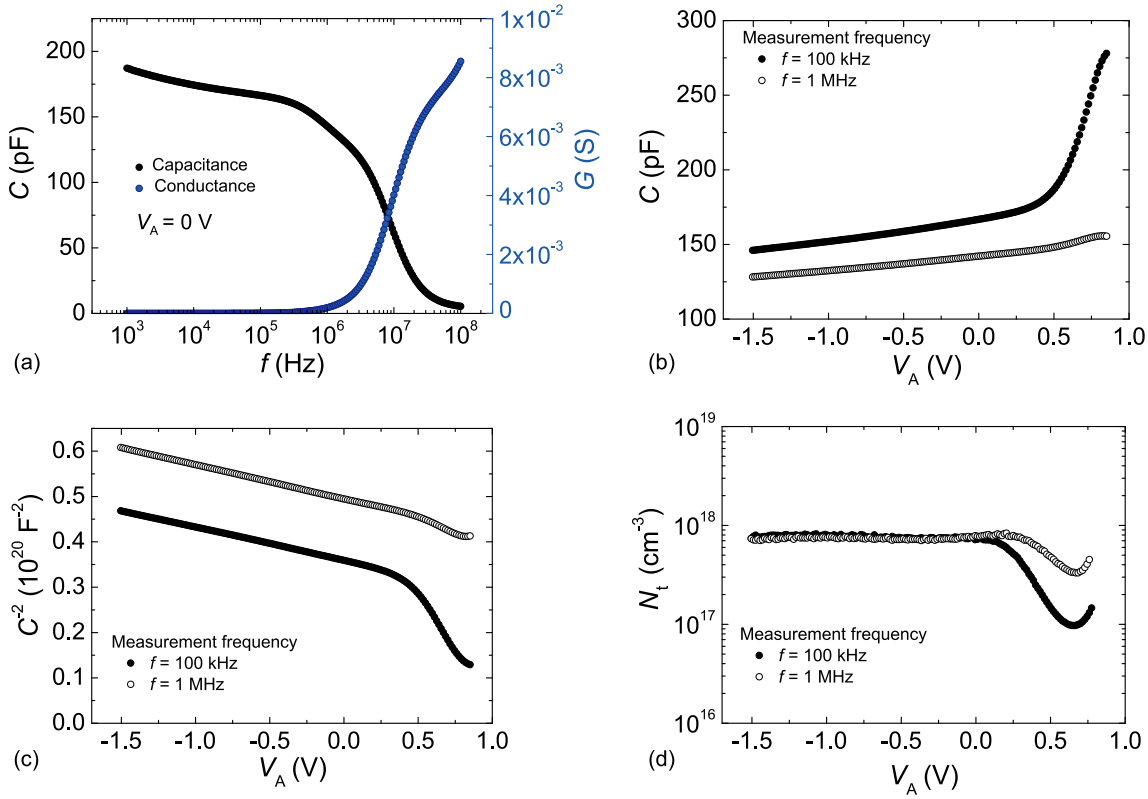

Figure 7 (a) Capacitance (left axis) and conductance (right axis) in dependence on the frequency of a Cu/Ga_2O_3 SC on a sample with f-b geometry. The external bias for this measurement was zero. (b) Capacitance in dependence on the applied voltage of a Cu/Ga_2O_3 SC with a f-b geometry for measurement frequencies of $f = 100\,\mathrm{kHz}$ and $f = 1\,\mathrm{MHz}$. (c) C^{-2} in dependence on the applied voltage. (d) Net doping density in dependence on the applied voltage. (c) and (d) are calculated from the capacitance-voltage measurements visualized in (b). All measurements were performed at room temperature.

$f = 100\,\mathrm{kHz}$ and $f = 1\,\mathrm{MHz}$. Starting at negative applied voltages, the capacitance increases with increasing voltage, because the width of the space charge region of the SC decreases. The measured capacitance for the measurement at a frequency of $f = 1\,\mathrm{MHz}$ is smaller due to the frequency dependence of the capacitance shown in Fig. 7(a). Also, the relative change of the capacitance for this measurement is smaller than for the measurement at $f = 100\,\mathrm{kHz}$, indicating an additional frequency dependent effect. According to [25] the dependence of the capacitance of a SC on the applied voltage is

$$C = A_0 \sqrt{\frac{N_\mathrm{t}\epsilon_\mathrm{s}\epsilon_0}{2(eV_\mathrm{bi} - eV_\mathrm{A} - k_\mathrm{B}T)}}\,. \tag{9}$$

Therefore, by plotting C^{-2} in dependence on the applied voltage, it is expected that the extrapolation of C^{-2} to zero yields V_bi. In Fig. 7(c) such a plot is shown for the measured data from Fig. 7(b) for both measurement frequencies. The plot deviates from the linear dependency for applied voltages larger than $0\,\mathrm{V}$. Additionally, the intersection point varies strongly with the measurement frequency, therefore, the estimation of the built-in voltage is not reasonable here. This behaviour is likely to be due to deep traps as discussed in the following.

According to Eq. (9) the net doping concentration can be calculated from the measured data using the derivative of C^{-2} with respect to the applied voltage

$$N_\mathrm{t}(w) = -\frac{2}{eA_0^2\epsilon_\mathrm{s}\epsilon_0}\left(\frac{\mathrm{d}}{\mathrm{d}V_\mathrm{A}}C^{-2}\right)^{-1}\,. \tag{10}$$

In Fig. 7(d) the net doping concentration is plotted in dependence on the applied voltage. A plot of the net doping concentration in dependence on the width of the space charge region is not useful here since the capacitance is strongly dependent on the measurement frequency and, therefore, would result in different doping profiles for different frequencies. From Fig. 7(d) we can determine the net doping concentration in the β-Ga_2O_3 thin film to be constant at a value of $N_\mathrm{t} = 8 \times 10^{17}\,\mathrm{cm}^{-3}$ for negative applied voltages (large width of the space charge region, net doping density in the bulk). This value is in good agreement with the value obtained by the fit of the I-V characteristics at high temperatures with the TE model taking image force lowering into account. For applied voltages larger

than zero, which is equivalent to a small space charge region and with that a measure of the net doping density near the surface of the thin film, the calculated net doping concentration decreases. This is the same as seen previously in Fig. 7(b) and (c) for the same voltage range. Since it is dependent on the measurement frequency, its is unlikely to be due to a decrease in the net doping and hence due to another effect. As shown by Kimerling [29] such a behaviour of the net doping profile can be assigned to a deep trap state with concentration N_T in the semiconductor. According to this theory, the value of the calculated net doping starts at N_t or $N_\mathrm{t} - N_\mathrm{T}$ near the surface of the semiconductor ($V_\mathrm{A} > 0$) and turns into $N_\mathrm{t} + N_\mathrm{T}$ or N_t in the bulk of the semiconductor in presence of a deep donor or acceptor trap, respectively. Since the calculated net doping density near the surface of the semiconductor is frequency dependent, it is likely that the trap state in our sample is a deep acceptor.

4 Conclusion In conclusion, we have demonstrated the fabrication of Cu SCs on heteroepitaxial β-Ga_2O_3 thin films on sapphire substrates. The electronic properties of those SCs were investigated by means of measuring I-V characteristics and determination of the effective barrier height and the ideality factor. The best SCs had effective barrier heights between $0.88\,\mathrm{eV}$ and $0.95\,\mathrm{eV}$ and ideality factors in the range of 1.2 to 1.4 at room temperature. By using an ohmic ZnO:Ga back contact layer, the series resistance could be reduced by two orders of magnitude in comparison to the SCs with a front-to-front contact geometry to several $100\,\Omega$. Temperature-dependent measurements showed that the effective barrier height depends linearly on the inverse temperature in accordance to thermionic emission theory over a laterally inhomogeneous barrier with a mean barrier height of $1.32 \pm 0.05\,\mathrm{eV}$ and standard deviation of $126 \pm 10\,\mathrm{meV}$. From measurements at high temperatures the effective barrier height for an ideality factor of 1.03 was determined to be $1.36\,\mathrm{eV}$ at $550\,\mathrm{K}$, which is in good agreement with the mean barrier height determined at lower temperatures ($110\,\mathrm{K}$-$320\,\mathrm{K}$). Consistently, the reverse current for high temperatures can be described by thermionic emission theory considering image force lowering. Thus, the SC is stable up to at least $550\,\mathrm{K}$ and electrically close to ideal at this temperature. The low series resistance also enabled us to perform C-V measurements at high frequencies, but due to a deep trap in the semiconductor, an estimation of the built-in voltage from the C-V-measurement was not possible. Nevertheless, the net doping concentration was estimated to be $N_\mathrm{t} = 8{\times}10^{17}\,\mathrm{cm}^{-3}$.

5 Acknowledgements We thank H. Hochmuth for PLD growth of the investigated thin films, G. Ramm for the preparation of the PLD targets and M. Hahn and Z. Zhang for the bonding of the contacts. This work was supported within the framework of EFRE (SAB 100132251) and by Universität Leipzig.

References

[1] M. Higashiwaki, K. Sasaki, A. Kuramata, T. Masui, and S. Yamakoshi, Appl. Phys. Lett. **100**(1), 013504 (2012).
[2] T. Oshima, T. Okuno, N. Arai, N. Suzuki, S. Ohira, and S. Fujita, Appl. Phys. Express **1**(1), 011202 (2008).
[3] R. Suzuki, S. Nakagomi, Y. Kokubun, N. Arai, and S. Ohira, Appl. Phys. Lett. **94**(22), 222102 (2009).
[4] K. Irmscher, Z. Galazka, M. Pietsch, R. Uecker, and R. Fornari, J. Appl. Phys. **110**(6), 063720 (2011).
[5] M. Mohamed, K. Irmscher, C. Janowitz, Z. Galazka, R. Manzke, and R. Fornari, Appl. Phys. Lett. **101**(13), 132106 (2012).
[6] K. Sasaki, M. Higashiwaki, A. Kuramata, T. Masui, and S. Yamakoshi, J. Cryst. Growth (2013), DOI: 10.1016/j.jcrysgro.2013.02.015.
[7] H. Aida, K. Nishiguchi, H. Takeda, N. Aota, K. Sunakawa, and Y. Yaguchi, Jpn. J. Appl. Phys. **47**(11), 8506–8509 (2008).
[8] S. Müller, H. von Wenckstern, D. Splith, F. Schmidt, and M. Grundmann, Phys. Status Solidi A (in print), doi: 10.1002/pssa.201330025 (2013).
[9] H. v. Wenckstern, G. Biehne, R. A. Rahman, H. Hochmuth, M. Lorenz, and M. Grundmann, Appl. Phys. Lett. **88**(9), 092102 (2006).
[10] E. G. Villora, K. Shimamura, T. Ujiie, and K. Aoki, Appl. Phys. Lett. **92**(20), 202118 (2008).
[11] A. Lajn, H. v. Wenckstern, M. Grundmann, G. Wagner, P. Barquinha, E. Fortunato, and R. Martins, J. Appl. Phys. **113**(4), 044511 (2013).
[12] C. R. Crowell and S. M. Sze, Solid-State Electron. **9**(11–12), 1035–1048 (1966).
[13] H. He, R. Orlando, M. Blanco, R. Pandey, E. Amzallag, I. Baraille, and M. Rérat, Phys. Rev. B **74**(19) (2006).
[14] J. H. Werner and H. H. Güttler, J. Appl. Phys. **69**(3), 1522–1533 (1991).
[15] R. F. Schmitsdorf and W. Mönch, EPJ B **7**(3), 457–466 (1999).
[16] M. Orita, H. Hiramatsu, H. Ohta, M. Hirano, and H. Hosono, Thin Solid Films **411**(1), 134–139 (2002).
[17] K. Matsuzaki, H. Yanagi, T. Kamiya, H. Hiramatsu, K. Nomura, M. Hirano, and H. Hosono, Appl. Phys. Lett. **88**(9), 092106 (2006).
[18] K. Matsuzaki, H. Hiramatsu, K. Nomura, H. Yanagi, T. Kamiya, M. Hirano, and H. Hosono, Thin Solid Films **496**(1), 37–41 (2006).
[19] S. Nakagomi and Y. Kokubun, J. Cryst. Growth **349**(1), 12–18 (2012).
[20] S. A. Lee, J. Y. Hwang, J. P. Kim, S. Y. Jeong, and C. R. Cho, Appl. Phys. Lett. **89**(18), 182906 (2006).
[21] K. Nakahara, T. Tanabe, H. Takasu, P. Fons, K. Iwata, A. Yamada, K. Matsubara, R. Hunger, and S. Niki, Jpn. J. Appl. Phys. Part 1 **40**(1), 250–254 (2001).
[22] M. Grundmann, T. Böntgen, and M. Lorenz, Phys. Rev. Lett. **105**(14), 146102 (2010).
[23] M. Grundmann, Phys. Status Solidi B **248**(4), 805–824 (2011).
[24] K. Momma and F. Izumi, J. Appl. Crystallogr. **44**(6), 1272–1276 (2011).

[25] M. Grundmann, The Physics of Semiconductors: An Introduction Including Nanophysics and Applications, 2 edition (Springer-Verlag, Berlin Heidelberg, 2010).
[26] M. W. Allen, X. Weng, J. M. Redwing, K. Sarpatwari, S. E. Mohney, H. von Wenckstern, M. Grundmann, and S. M. Durbin, IEEE Trans. Electron Dev. **56**(9), 2160–2164 (2009).
[27] M. Passlack, N. E. J. Hunt, E. F. Schubert, G. J. Zydzik, M. Hong, J. P. Mannaerts, R. L. Opila, and R. J. Fischer, Appl. Phys. Lett. **64**(20), 2715 (1994).
[28] J. Vancea, G. Reiss, D. Butz, and H. Hoffmann, Europhys. Lett. **9**(4), 379 (1989).
[29] L. C. Kimerling, J. Appl. Phys. **45**(4), 1839–1845 (1974).